slPCMlib: A Modelica Library for the Prediction of Effective Thermal Material Properties of Solid/Liquid Phase Change Materials (PCM)

Tilman Barz Aurelien Bres Johann Emhofer

Center for Energy, AIT Austrian Institute of Technology GmbH, Giefingasse 2, 1210 Vienna, Austria
tilman.barz@ait.ac.at

Abstract

slPCMlib predicts the effective thermal properties of solid/liquid phase change materials (PCM) showing a non-isothermal phase transition behavior. The effective properties are valid over the PCM functional temperature range where latent heat is absorbed and released. Different phenomenological phase transition models are implemented to account for temperature shifts in latent transition changes, e.g. due to multi-step transitions and thermal hysteresis. The library currently contains generic PCM and specific commercial paraffin-based and hydrated salt-based PCM (media). Its purpose is the analysis of partial and complete melting and solidification processes relevant for engineering applications, such as the design of PCM-enhanced building components.

Keywords: solid/liquid phase transition, thermal hysteresis, phase change material (PCM)

1 Introduction

Solid/liquid phase change materials (PCM), such as salt hydrates, paraffin waxes, fatty acids and eutectics of organic and non-organic compounds are used for storing thermal energy (heat or cold) and/or to regulate temperatures, in a small temperature range with high efficiency. Numerous applications are reported where PCM is incorporated in building envelopes (Al-Yasiri and Szabó, 2021; Kuznik et al., 2011).

***Ideal* versus *real* phase change behavior:** While *ideal* PCM show an isothermal phase change behavior, many *real* (commercial) PCM show a non-isothermal phase change behavior: they melt and solidify over an extended temperature range. Moreover, a large part of the PCM available for building applications shows thermal hysteresis (including supercooling), which can be measured by a (temperature) shift in the enthalpy curves for heating and cooling. This phenomenon additionally extends the temperature range where the latent heat is absorbed and released. Accordingly Kośny (2015) introduce the "PCM functional temperature range", which starts at the lowest temperature limit of the solidification process and ends at the highest temperature of the melting process. Figure 1 exemplifies different phase transition behavior of *ideal* and *real* PCM.

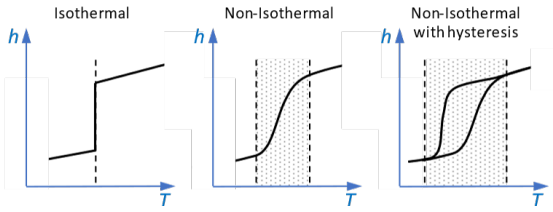

Figure 1. Enthalpy as a function of temperature for the case of an isothermal transition, a non-isothermal transition, and a non-isothermal transition with hysteresis.

The thermo-physical and rheological properties of PCM are usually characterized not only by the calorific properties, but also by the thermal conductivity in the solid and liquid phases, viscosity of liquid PCM and density as a function of temperature (Kośny, 2015). Considering *real* PCM these properties also change over the phase transition temperature range.

Phenomenological phase transition models: Although it has been recognized by many research groups that complex phase transition phenomena in *real* materials can have a significant impact on PCM performance, only few numerical models have been developed which are able to represent specific effects such as hysteresis and supercooling (Kośny, 2015).

Kośny (2015) review PCM modeling algorithms commonly used in building energy and hygrothermal software. The phase transition behavior is mostly characterized by a single enthalpy-temperature, or apparent heat capacity-temperature curve which can be obtained e.g. from caloric measurements. Corresponding models are purely data-driven, phenomenological models, which can be easily applied for the analysis of PCM showing non-isothermal and rate-independent phase transition phenomena (Barz et al., 2019). However, in most software the parametrization of the curve's shape is usually restricted. Only few software offer separate curves for melting and freezing (to account for thermal hysteresis).

Recently, different phenomenological thermal hysteresis models have been proposed: The so-called "curve track" model uses different curves for complete melting or solidification processes, e.g. (Michel et al., 2017; Biswas

et al., 2018; Moreles et al., 2018; Filonenko et al., 2020). The so-called "curve switch" model is an extension allowing minor loops relevant for incomplete (or interrupted) phase transitions, e.g. (Bony and Citherlet, 2007; Rose et al., 2009; Buonomano and Guarino, 2020; Goia et al., 2018; Hu and Heiselberg, 2018). Another extension is the so-called "curve scale" model, e.g. (Barz and Sommer, 2018; Barz et al., 2019; Barz, 2021; Lizana et al., 2021).

Modelling heat transfer in PCM: There exist different numerical modeling approaches to deal with the moving boundary between phases during melting and solidification. Considering *real* PCM, it seems most reasonable to adopt the so-called weak formulation, specifically the enthalpy method and apparent heat capacity method. Here, the explicit treatment of a moving interface is avoided, and instead, a mushy transition zone between the two phases is considered where effective enthalpy- or apparent heat capacity-temperature curves are applied, see Voller et al. (1990) for details.

For a recent literature review on Modelica implementations of numerical models for heat transfer in *ideal* and *real* PCM we refer to Helmns et al. (2021). As an example, Helmns et al. (2021) uses the enthalpy method as implemented in the Modelica Buildings Library (Wetter et al., 2014) for the development of a component model of a thermal energy storage with PCM. The heat conduction equation is formulated with the enthalpy (or internal energy) as dependent variable. The temperature is modeled as a piecewise linear function of enthalpy (inverse enthalpy-temperature relation), which is represented (approximately) by a cubic hermite spline interpolation. The enthalpy method allows for the solution of heat conduction problems in *real* and *ideal* PCM. In the Modelica Buildings Library generic PCM with an (almost) isothermal behavior use small phase transition temperature ranges of 0.02 K.

Leonhardt and Müller (2009); Halimov et al. (2019) use the apparent heat capacity method and extend AixLib, a Modelica model library for building performance simulations, by heat capacity-temperature relations for *real* PCM. Different curve shapes were experimentally validated for a commercial paraffin-based PCM using alternative temperature-dependent continuous ansatz functions, such as arctangent function (Halimov et al., 2019).

This contribution: A new library slPCMlib is presented which predicts effective properties of *real* PCM. It contains the above mentioned phenomenological phase transition (hysteresis) models as well as generic and specific PCM (media) for which the phase transition behavior was identified from caloric measurement data. Examples for conduction dominated heat transfer in PCM are presented adopting the apparent heat capacity method.

2 Effective material properties

The following assumptions are taken for modeling effective PCM properties:

- There are only two phases (two-phase model): a solid and a liquid phase.
- Phase transitions are induced by temperature and are independent of pressure.
- Phase transitions extend over a temperature range (non-isothermal phase transitions) and are continuous.
- Within the phase transition temperature range the solid and liquid phases coexist as a homogenous mixture (macroscopic view). The material is then in a semi-solid or semi-liquid state which produces a mushy zone in the PCM domain.
- Properties of the mushy state are local effective (also apparent) mixture properties, which are defined by a weighting of contributions from solid and liquid phases. The weighting is based on the phase change progress, i.e. the mass (or volume) phase fraction.

The effective enthalpy $h(T)$, density $\rho(T)$ and thermal conductivity $\lambda(T)$ are calculated as[1]:

$$h(T) = (1-\xi(T))\, h^s(T) + \xi(T)\, h^l(T) \tag{1a}$$

$$\rho(T) = (1-\phi(T))\, \rho^s(T) + \phi(T)\, \rho^l(T) \tag{1b}$$

$$\lambda(T) = (1-\phi(T))\, \lambda^s(T) + \phi(T)\, \lambda^l(T) \tag{1c}$$

where $\xi(T)$ and $\phi(T)$ are the liquid mass and liquid volume phase fraction, respectively[2]. Their relation is:

$$\phi(T) = \frac{\xi(T)}{\xi(T) + (1-\xi(T))\frac{\rho^l(T)}{\rho^s(T)}} \tag{2}$$

The apparent specific heat capacity $\tilde{c}(T) = dh(T)/dT$ reads:

$$\tilde{c}(T) = \underbrace{(1-\xi(T))\, c_p^s(T) + \xi(T)\, c_p^l(T)}_{\text{baseline, } c_{\mathrm{BL}}(T)} + \underbrace{\frac{d\xi}{dT}\left(h^l(T) - h^s(T)\right)}_{\text{peak function}} \tag{3}$$

It is assumed that the properties of the single phases ρ^l, ρ^s, λ^l, λ^s, and c_p^l, c_p^s are available. The difference in solid and liquid enthalpies h^l, h^s defines the phase transition enthalpy. For non-isothermal transitions there exist different approaches for the calculation. They are linked with the method for determining the phase transition function $\xi(T)$. The determination of $\xi(T)$ and $h^l(T)$, $h^s(T)$ are discussed in the following.

[1] While viscosity is also an important property it is not considered as effective variable here. The reason is that in numerical modeling viscosity in the solid is usually either neglected or artificially increased to ensure zero velocity fields in the solid phase. However, liquid viscosity might be considered by extending basic PCM properties in `slPCMlib.Media` discussed in Section 4.1.

[2] For better readability the symbols ξ and ϕ have no superscript (l) to indicate liquid phase fraction. Obviously, considering two components the solid phase fractions read $1-\xi(T)$ and $1-\phi(T)$.

DOI 10.3384/ecp19363

2.1 Phase transition functions for heating and cooling

Phase transition functions describe the phase change progress for complete transitions during heating (complete melting with $dT/dt > 0$), and for complete transitions during cooling (complete solidification with $dT/dt < 0$), respectively. Note that, because the behavior might be different for melting and solidification (thermal hysteresis), two different transition functions are considered:

$$\begin{aligned} \xi^H &= \xi(T) \quad \text{for heating} \\ \xi^C &= \xi(T) \quad \text{for cooling} \end{aligned} \tag{4}$$

It is assumed that: The transition functions:

- depend on temperature, are differentiable and monotonically increase with rising temperature.
- realize a transition from $\xi = 0$ (solid) to $\xi = 1$ (liquid).
- are shifted in temperature (thermal hysteresis) and do not intersect: $\xi^H(T) \leq \xi^C(T) \; \forall \, T$.

The limits of the phase transition temperature are defined as:

$$\begin{aligned} T_{\min} &= \max\{T \,|\, \xi(T) = 0\} \\ T_{\max} &= \min\{T \,|\, \xi(T) = 1\} \end{aligned} \tag{5}$$

Because of the assumption above, in case of thermal hysteresis $T_{\min}$ corresponds to ξ^C, and $T_{\max}$ to ξ^H. This means that the phase transition temperature range (also PCM functional temperature range) starts at $T_{\min}$ of the solidification process, and ends at $T_{\max}$ of the melting process. Examples for the transition functions are shown in Figure 3 (bottom).

2.2 Determination of phase transition functions and single phase enthalpies

The heat storage capacity of PCM is usually tabulated as scalar values for the phase change enthalpy and melting temperature. For some PCM also apparent heat capacity curves are available, e.g. Figure 2. As pointed out e.g. by Kośny (2015), a *real* PCM with a non-isothermal phase change behavior should be represented by a temperature dependent function, e.g. $h(T)$.

In Differential Scanning Calorimetry (DSC) analysis, which is a standard technique for caloric measurements of PCM, the (*scalar*) phase transition enthalpy Δh_t is usually determined as the area between two curves defined in Equation (3): the apparent (effective) heat capacity $\tilde{c}(T)$, and the baseline heat capacity $c_{\mathrm{BL}}(T)$ (Hemminger and Sarge, 1991).

$$\Delta h_t = \int_{T_{\min}}^{T_{\max}} (\tilde{c}(\tau) - c_{\mathrm{BL}}(\tau))\, d\tau \tag{6}$$

The baseline $c_{\mathrm{BL}}(T)$ connects solid and liquid heat capacities in the phase transition temperature range and is determined by a suitable baseline construction method. After

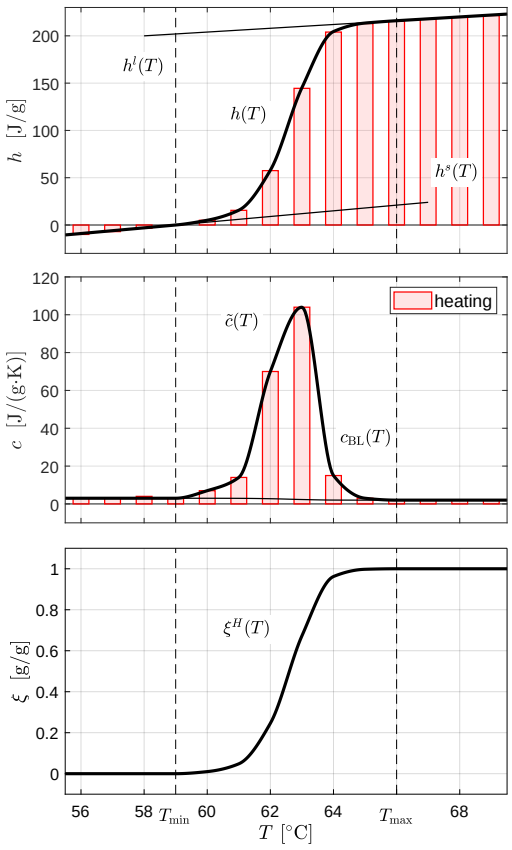

Figure 2. Determination of the phase transition function for heating and the single phase enthalpies from heat capacity data of RT62HC. Middle: The bars depict the data as provided by the PCM manufacturer (Rubitherm Technologies GmbH). The data (partial enthalpies for one Kelvin intervals) was collected using a three-layer-calorimeter. The lines depict the fitted effective heat capacity, see Barz et al. (2020) for details. Top: Derived enthalpy data. Bottom: Derived phase transition function for heating.

substraction of the baseline, the phase transition function is obtained from the cumulative integral over the normalized peak, taking $T_{\min}$ and $T_{\max}$ as integration limits.

For *ideal* PCM with an isothermal phase change behavior, the *scalar* Δh_t in Equation (6) is the transition enthalpy at a reference temperature, i.e. the melting temperature. For *real* PCM (considered in this contribution), Δh_t is *temperature dependent*. The dependence is given by the so-called Kirchhoff equation (or Kirchhoff's Law), which relates the isobaric temperature variation of the phase transition enthalpy to the difference in specific heat capacities at constant pressure (McDonald, 1953):

$$\left.\frac{\partial \Delta h_t}{\partial T}\right|_p = c_p^l - c_p^s \tag{7}$$

The Kirchhoff equation yields a *temperature-dependent* phase transition enthalpy, which is used in Equation (3) in the peak function:

$$\Delta h_t(T) = h^l(T) - h^s(T) \tag{8}$$

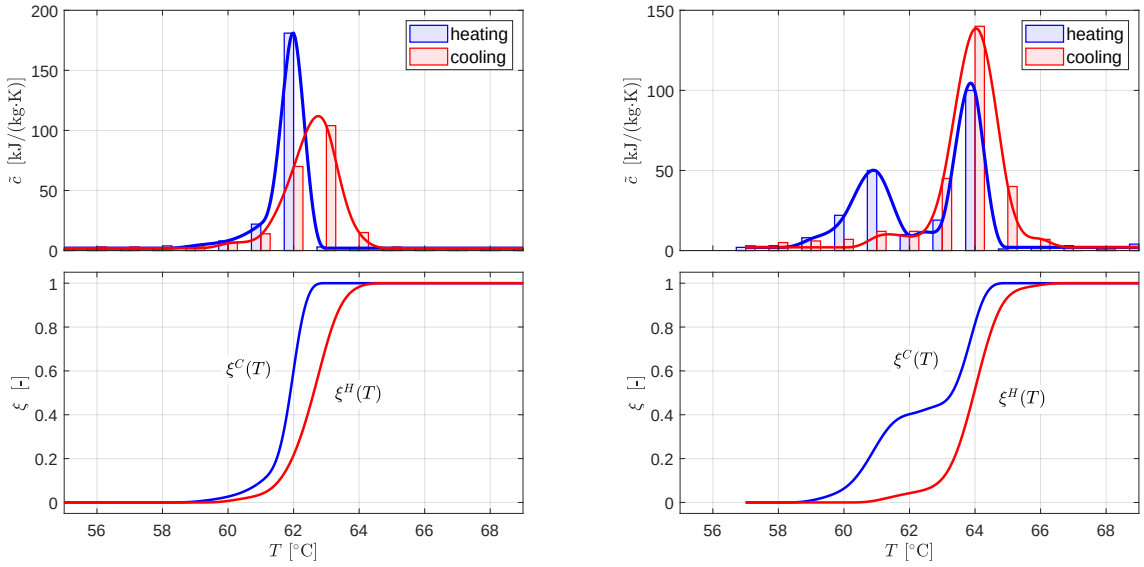

Figure 3. Determination of phase transition functions for heating ξ^H and cooling ξ^C from heat capacity data of Rubitherm RT62HC (left) and RT64HC (right), see Barz et al. (2020) for details. Top: The bars depict heat capacity data provided by the PCM manufacturer (Rubitherm Technologies GmbH). The data (partial enthalpies) were recorded using a three-layer-calorimeter. The lines depict the fitted effective heat capacity. Bottom: Derived phase transition functions.

In slPCMlib the *single phase* solid and liquid enthalpies are defined as:

$$h^s(T) = h^s(T_{\text{ref}}) + \int_{T_{\text{ref}}}^{T} c_p^s(\tau)d\tau \tag{9a}$$

$$h^l(T) = h^l(T_{\text{max}}) + \int_{T_{\text{max}}}^{T} c_p^l(\tau)d\tau \tag{9b}$$

with $T_{\text{ref}} \leq T_{\text{min}}$ and

$$h^s(T_{\text{ref}}) = h_{\text{ref}} \tag{10a}$$

$$h^l(T_{\text{max}}) = h_{\text{ref}} + \int_{T_{\text{ref}}}^{T_{\text{max}}} c_{\text{BL}}(\tau)d\tau + \Delta h_t \tag{10b}$$

To briefly sum up, the following definitions are used:

- Δh_t is the *scalar* phase transition enthalpy for melting of a *real* PCM with a non-isothermal phase change behavior. It is defined for the *melting temperature range* (not the melting temperature), and it is determined from heat capacity data for heating using Equation (6) .
- $\Delta h_t(T) = h^l(T) - h^s(T)$ is the *temperature dependent* phase transition enthalpy. The single phase enthalpies h^l and h^s are computed via Equation (10) for a given *scalar* Δh_t.

Enthalpy $h(T)$ and apparent heat capacity $\tilde{c}(T)$ are calculated considering the temperature dependent transition enthalpy in Equation (8) and Equations (1a) and (3).

Note that, if heat capacity data for melting and solidification is different (thermal hysteresis), then the phase transition functions for melting ξ^H and solidification ξ^C are determined for each data set independently, see Figure 3 for examples. However, the *scalar* phase transition enthalpy Δh_t is obtained from the data for melting. In some cases it might by necessary to adapt the value of Δh_t in order to generate a "best fit" for both data sets.

3 Phase transition models

In addition to the assumptions in Section 2, the following assumption is used for modeling the phase transition behavior for melting and solidification processes:

- Phase transitions are rate-independent (equilibrium model).

It follows that, increased heating or cooling rates lead to faster melting and solidification. However, the rate has no effect on the systems behavior itself. The graphs in the (ξ, T)-plane and the (h, T)-plane are unchanged. For the hysteresis models discussed in the following, this means that also the magnitude of the hysteresis is rate-independent.

3.1 The *melting curve* model

The simplest model (here referred to as *melting curve* model) predicts the evolution of the phase fraction as response to arbitrary changes in temperature using the phase transition function for heating:

$$\xi = \xi^H(T) \tag{11}$$

The model does not account for hysteresis phenomena, see Figure 4 for an example.

3.2 The *curve track* hysteresis model

The *curve track* hysteresis model predicts the evolution of the phase fraction as response to positive or negative

DOI
10.3384/ecp19363

changes in temperature T, starting from T_0 to the final value T_f, using one of the following submodels:

$$\xi(T) = \xi^H(T) \quad \text{if} \quad T_0 = T_{\min} \tag{12a}$$
$$\xi(T) = \xi^C(T) \quad \text{if} \quad T_0 = T_{\max} \tag{12b}$$

where T_0 is the discrete (piecewise constant) temperature which changes only when T crosses the limits of the phase transition temperature range. At this point the final variable T_f is reached, the process is restarted setting $T_0 = T_f$ and choosing the next submodel. This means that T_0 holds the information which transition (melting or solidification) was completed last, e.g. $T_0 = T_{\min}$ means that the PCM was in the complete solid state and the heating curve $\xi^H(T)$ is currently used.

The *curve track* model is completely defined by $\xi^H(T)$ and $\xi^C(T)$, and the limits $T_{\min}$ and $T_{\max}$. The model is useful for the prediction of complete melting or complete solidification processes. The model is not useful for incomplete phase transition processes. This is because switches between heating and cooling, while the material is still within the phase transition range, do not result in a change (e.g. switch) of the phase transition function, see (Barz et al., 2019). An example for complete and incomplete melting and solidification processes is shown in Figure 4.

3.3 The *curve switch* hysteresis model

The *curve switch* model, first proposed by Bony and Citherlet (2007), extends the *curve track* model for an improved prediction of interrupted phase transitions, i.e. incomplete transitions with switches between heating and cooling. Incomplete transitions are modeled by a straight line between the phase fraction-temperature curves (and enthalpy–temperature curves) for heating and cooling. Following this connecting line realizes the so-called *curve switch*.

The evolution of the phase fraction as response to positive or negative changes in T, starting at T_0 and ending at T_f is described by three submodels for melting, soldification and the curve switch:

$$\xi(T) = \xi^H(T) \quad \text{if} \quad T_0 = T_{\min} \tag{13a}$$
$$\xi(T) = \xi^C(T) \quad \text{if} \quad T_0 = T_{\max} \tag{13b}$$
$$\xi(T) = \text{constant} \quad \text{if} \quad T_{\min} < T_0 < T_{\max} \tag{13c}$$

where, in the same way as in Equation (12), T_0 is the discrete (piecewise constant) temperature indicating which submodel is used. The following conditions can trigger an event (T_f is reached): When T crosses the limits of the phase transition temperature range, then either $T_f = T_{\min}$ or $T_f = T_{\max}$; During melting or solidification with $T_{\min} < T < T_{\max}$, when the temperature rate dT/dt changes the sign, then $T_f = T$ (initiation of curve switch); During the curve switch, when $\xi(T)$ reaches either the curve for heating $\xi(T) = \xi^H(T)$ or cooling $\xi(T) = \xi^C(T)$, then either $T_f = T_{\min}$ or $T_f = T_{\max}$ (finalization of curve switch).

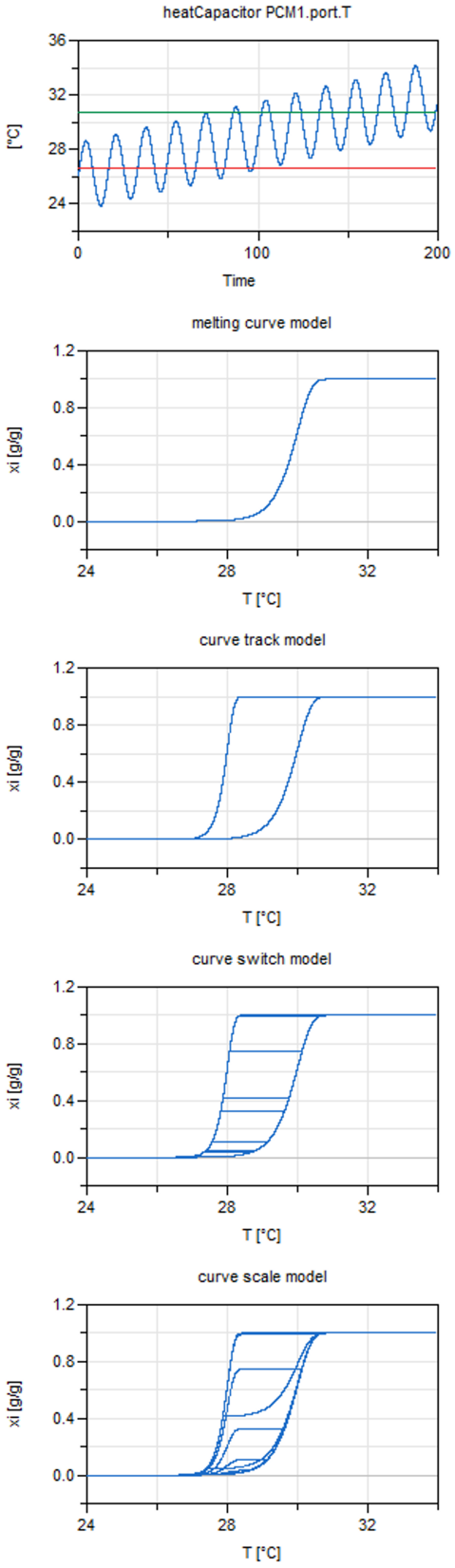

Figure 4. Evolution of the phase fraction as response to sinusoidal temperature variations considering different rate-independent phase transition models. The first subfigure shows the temperature input and the limits of the phase transition temperature range. The following subfigures show the corresponding responses in the (T, ξ)-plane. Note that, since the hysteresis models are static models, time is given in arbitrary unit.

When T_f is reached the process is restarted setting $T_0 = T_f$ and choosing the next submodel.

The *curve switch* model is completely defined by $\xi^H(T)$ and $\xi^C(T)$, and the limits $T_{\min}$ and $T_{\max}$. For complete melting and solidification the model produces the same results as the *curve track* model. An example is shown in Figure 4.

3.4 The *curve scale* hysteresis model

The *curve scale* model, originally introduced by Ivshin and Pence (1994) for the modeling of temperature induced phase transitions and first applied by Barz and Sommer (2018) in the context of solid/liquid PCM, is another extension of the *curve track* model. The model accounts for different hysteresis magnitudes for cycles within the phase transition temperature range and makes use of the temperature history. Major and minor hysteresis loops are constructed by scaling the functions for complete transitions $\xi^H(T)$ and $\xi^C(T)$.

The evolution of the phase fraction as response to a monotonous change in T from a starting value T_0 to the final value T_f is described by two submodels:

$$\xi(T) = 1 - s^{\text{pos}} \cdot \left(1 - \xi^H(T)\right) \quad \text{if} \quad dT/dt \geq 0 \tag{14a}$$

$$\xi(T) = s^{\text{neg}} \cdot \xi^C(T) \quad \text{if} \quad dT/dt < 0 \tag{14b}$$

with the scaling factors:

$$s^{\text{pos}} = \frac{1-\xi_0}{1-\xi^H(T_0)}, \qquad s^{\text{neg}} = \frac{\xi_0}{\xi^C(T_0)} \tag{15}$$

where T_0 and $\xi_0 := \xi(T_0)$ denote the initial temperature and phase fraction for time intervals with either increasing or decreasing temperatures. Thus, during monotonically increasing (or decreasing) temperatures all variables in Equation (15) are constant. Their values are updated only at time instants (events) when the sign of dT/dt changes.

An equivalent differential form of the curve scale hysteresis model is obtained by differentiation of Equations (14), (15) with respect to time using the chain rule (Ivshin and Pence, 1994):

$$\frac{d\xi}{dt} = \frac{1-\xi(T)}{1-\xi^H(T)} \cdot \frac{d\xi^H(T)}{dT} \cdot \frac{dT}{dt} \quad \text{if} \quad \frac{dT}{dt} \geq 0 \tag{16a}$$

$$\frac{d\xi}{dt} = \frac{\xi(T)}{\xi^C(T)} \cdot \frac{d\xi^C(T)}{dT} \cdot \frac{dT}{dt} \quad \text{if} \quad \frac{dT}{dt} < 0 \tag{16b}$$

With this modification the discrete (piecewise constant) variables in Equation (15) are replaced by continuous variables. It turns out that the model can be implemented as one differential equation with a discontinuous right hand side.

The *curve scale* model is completely defined by $\xi^H(T)$ and $\xi^C(T)$. For complete melting and solidification it produces the same results as the curve track model. Results for incomplete melting and solidification are shown in Figure 4.

4 Implementation in Modelica

An overview of the packages contained in slPCMlib is given in Figure 5.

4.1 Definition of media

The package `slPCMlib.Media` (see Figure 5) contains *specific* PCM data of commercial organic and inorganic PCM for which solid and liquid properties are tabulated and heat capacity curves are available in the technical data sheets provided by manufacturers. In addition, the package also contains four examples with *generic* PCM data, which can be adapted by the user to match a certain peak shape.

Each medium (PCM) extends the partial package `slPCMlib.interfaces.partialPCM` which contains the basic definition of a medium. Functions for *single phase* solid and liquid densities $\rho^s(T)$, $\rho^l(T)$ and thermal conductivities $\lambda^s(T)$, $\lambda^l(T)$) can be arbitrary functions of temperature. They are defined by a `replaceable partial function`. In contrast, functions for *single phase* heat capacities c_p^l, c_p^s are assumed to be linear functions of temperature: $a + b \cdot (T - T_{\text{ref}})$. Corresponding coefficients a, b, reference temperature T_{ref}, as well as reference enthalpy $h_{\text{ref}} = h(T_{\text{ref}})$, *scalar* phase transition enthalpy Δh_t, and the limits of the phase transition temperature range are defined in a replaceable record called `propData`.

4.1.1 Functions for heating and cooling

In the package `slPCMlib.Media` (see Figure 5) each PCM extends (replaceable partial) phase transition functions for heating and cooling, see Equation (4), contained in `slPCMlib.interfaces.partialPCM`.

```
replaceable partial function
↪phaseFrac_complMelting "Returns liquid
    mass phase fraction for complete
    melting processes"
  extends Modelica.Icons.Function;
  input Modelica.Units.SI.Temperature T;
  output Modelica.Units.SI.MassFraction xi;
  output Real dxi(unit="1/K");
end phaseFrac_complMelting;
```

The functions of the *specific* PCM are piecewise interpolation splines, see Barz et al. (2020) for details and Figures 3 (bottom) for examples. They are evaluated using e.g. `slPCMlib.BasicUtilities.quartQuintSplineEval`.

The four *generic* PCM use different ansatz functions. These are the uniform cumulative distribution function (CDF), the Gumbel Minimum (also Extreme value type I) CDF, the Gaussian (also Normal) CDF, and the 7th-order smoothstep function, shown in Figure 6 (top).

The uniform and Gaussian distribution are contained in `Modelica.Math.Distributions`, the Gumbel distribution extends this package and is implemented together with the smoothstep in `slPCMlib.BasicUtilities`.

DOI 10.3384/ecp19363

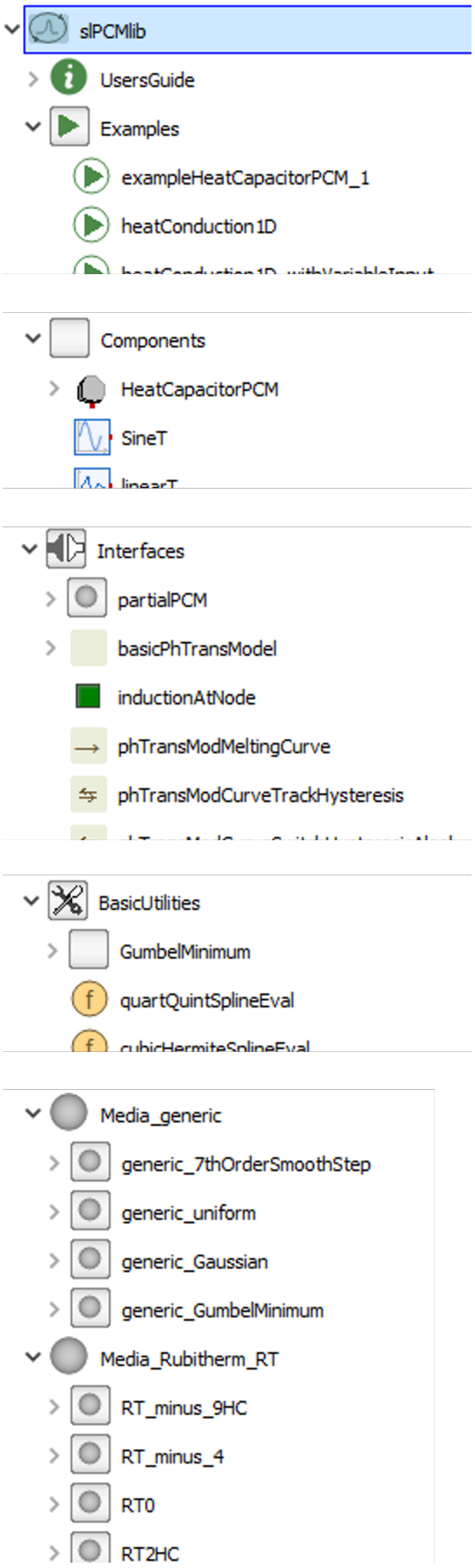

Figure 5. Packages in slPCMlib.

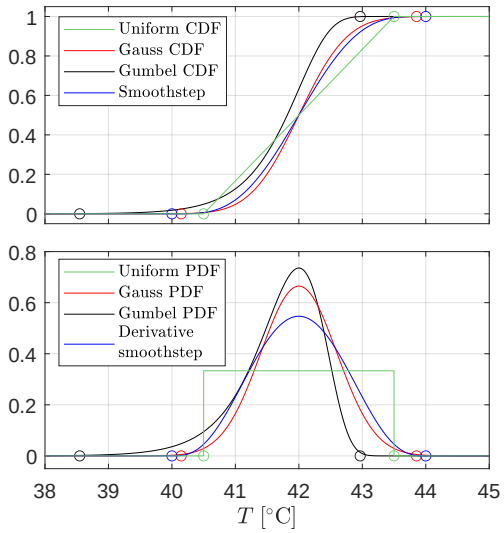

Figure 6. Ansatz functions used for the parametrization of *generic* PCM. Top: Examples for phase transition functions (either for heating or cooling). The following parameters have been used: $T_{\min} = 40.5$, $T_{\max} = 43.5$ (uniform); $\mu = 42$, $\beta = 0.5$ (Gumbel); $\mu = 42$, $\sigma = 0.6$ (Gauss); $T_{\min} = 40$, $T_{\max} = 44$ (Smoothstep). The circle indicates the (approximate in case of Gumbel and Gauss) start and end of the transition range. Bottom: Derivative w.r.t. temperature.

The derivatives of these ansatz functions represent the peak in the effective heat capacity, see also Equation (3) and Figure 6 (bottom). The asymmetric Gumbel distribution can be especially useful for the fitting of heat capacity data for cooling. The symmetric smoothstep function can be parametrized intuitively as it's so-called edge parameters coincide with $T_{\min}$ and $T_{\max}$. Because the CDF of Gumbel and Gauss distributions only asymptotically reach 0 and 1, the limits of the transition range are approximately set for the probabilities $P(T_{\min}) = 0.001$ and $P(T_{\max}) = 0.999$.

4.2 Computation of effective properties

Equations (1) - (3) are contained in the partial model `slPCMlib.Interfaces.basicPhTransModel`. The integral in Equation (10b) is computed by numerical integration using the function `Modelica.Math.Nonlinear.quadratureLobatto` within the `initial equation` section of `basicPhTransModel`. Because the *single phase* heat capacities are modeled as linear functions of temperature, the integrals in the formulas for the corresponding enthalpies in Equation (9b) can be solved analytically. The functions for the heat capacities, baseline and enthalpies are contained in `slPCMlib.BasicUtilities`.

4.3 Phase transition models

The phase transition models described in Section 3 are contained in `slPCMlib.Interfaces`, see Figure 5. They extend the `slPCMlib.Interfaces.basicPhTransModel`. The hysteresis models in Sec-

tion 3.2 - 3.4 are implemented using when-statements and discrete-time variables. As an example, the *curve track* model in Equation (12) uses the `discrete Boolean heatingOn` to hold the information which submodel is used. Events are triggered and the value of `heatingOn` is updated when T enters the phase transition temperature range, either crossing $T_{\min}$ with rising T, or when crossing $T_{\max}$ with falling T.

```
algorithm
  when (indVar.T <
      PCM.propData.rangeTmelting[2]) then
      ↪heatingOn := false;
  end when;
  when (indVar.T >
      PCM.propData.rangeTsolidification[1])
      ↪then heatingOn := true;
  end when;
```

In the same way, the *curve switch* model in Equation (13) uses the `discrete Integer modelInd` which can take the values +1 (Equation (13a)), -1 (Equation (13b)), and 0 (Equation (13c)).

The algebraic version of the *curve scale* model in Equations (14), (15) use `discrete Real` variables which are initialized and updated using the operator `pre()`. The following code fragment illustrates the updating of the scaling factor for heating:

```
algorithm
  when (indVar.der_T > 0) then
    T0  := pre(indVar.T);
    Xi0 := pre(xi_m);
    (Xi_at_T0,) :=
    ↪PCM.phaseFrac_complMelting(T0);
    scaler := (1.0-Xi0)
    ↪/max((1.0-Xi_at_T0),eps);
    heatingOn := true;
  end when;
```

In addition, several measures were taken to improve the robustness, performance and accuracy of the models:

- The *curve switch* and *curve scale* model are differentiated to avoid nonlinear algebraic equations. Note that for the *curve scale* model there are two versions available, one uses the algebraic formulation (Equation (14)) and the other uses the differential formulation (Equation (16a)).
- The states of the differentiated models are reinitialized at certain points where the exact solution is known. E.g. when the temperature passes the limits of the phase transition temperature range, the phase fraction is reinitialized either with zero or one.
- Additional conditions are considered in when-statements to reduce the number of events. E.g. in the *curve scale* model events are not triggered upon switches between heating and cooling outside the phase transition temperature range.

The following code fragment gives an example for the second point:

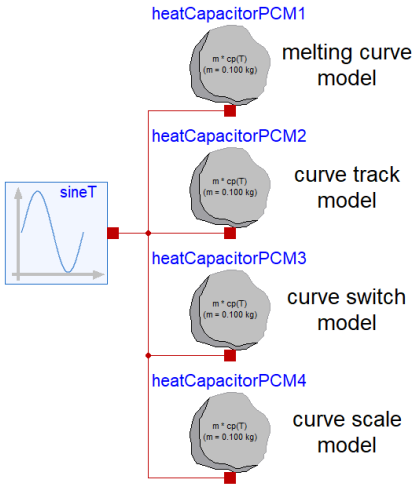

Figure 7. Diagram layer with the modified heat capacitor for the generation of the simulated data in Figure 4.

```
when (indVar.T <= PCM.propData.
↪rangeTsolidification[1]) then
  reinit(xi, 0.0);
elsewhen (indVar.T >= PCM.propData.
↪rangeTmelting[2]) then
  reinit(xi, 1.0);
end when;
```

4.4 Linking transition models and Media

In the following, the selection and use of a transition model and a PCM (medium) is discussed for a simple component model assuming homogenous temperatures inside the PCM. The Modelica Standard Library `heatCapacitor` contained in `Modelica.Thermal.HeatTransfer` has been modified to account for a temperature-dependent specific heat capacity. The modified capacitor `slPCMlib.Components.HeatCapacitorPCM` is shown in Figure 7. A PCM and a phase transition model are selected as:

```
replaceable package PCM=
  slPCMlib.Media.generic_GumbelMinimum;
replaceable slPCMlib.Interfaces.
↪phTransModCurveScaleHysteresis
    phTrModel(PCM=PCM);
```

In the equation section the temperature of the heat port of the capacitor `T` and it's derivative `der_T` are connected with the *inducing* port of the phase transition model `phTrModel.indVar`. The heat flow rate over the port of the capacitor `port.Q_flow` is calculated considering the temperature-dependent heat capacity:

```
equation
  T = port.T;
  der_T = der(port.T);
  phTrModel.indVar.T = T;
  phTrModel.indVar.der_T = der_T;
  phTrModel.cp*m*der(port.T) = port.Q_flow;
```


DOI
10.3384/ecp19363

5 Application examples

5.1 Partial phase transitions

Partial (or interrupted) phase transitions are common in PCM applications. They are characterized by switches between heating and cooling within the phase transition temperature range. Relevant scenarios are interrupted melting and subsequent cooling, or interrupted solidification and subsequent heating.

Figure 8 shows periodic temperature variations and responses in the enthalpy-temperature diagram for two different PCM. Results have been computed with the modified capacitor `HeatCapacitorPCM` choosing the "curve scale" model. The temperature first sweeps the full phase transition range, and subsequently the amplitude is reduced and the temperature oscillates within the transition range. It can be seen that the PCM undergo first a complete melting and solidification cycle forming a major loop. Subsequently, the enthalpy approaches the limit cycle (minor loop with partial transitions) where the absorbed and released heat is reduced. Figure 9 shows the corresponding density changes for both PCM.

5.2 Heat transfer in PCM

This example studies 1D heat conduction in a commercial PCM impregnated gypsum board, namely the SmartBoard®26 (SB26) manufactured by Knauf Gips KG, Germany. The interior plasterboard product with around 30 % mass fraction of microencapsulated paraffinic PCM is available for drywall construction applications in buildings (Kośny, 2015).

A package with the effective thermal properties of SB26 is contained in `Buildings.HeatTransfer.Data.SolidsPCM`. The phase transition function is modeled as piecewise linear function assuming a nearly isothermal phase change behavior. The transition range of this *ideal* SB26 is [25.99 °C, 26.01 °C].

Another package with effective properties of SB26 is contained in `slPCMlib.Media_Knauf_SmartBoard`. It uses the same single phase properties and phase transition enthalpy. However, two different phase transition functions for heating and cooling are considered (hysteresis). The transition functions were determined from heat capacity data published in Lerche et al. (2010) and are modeled by piecewise interpolation splines. The extended transition range of this *real* SB26 is [20 °C, 30 °C].

The SB26 wall element is modeled using the `Buildings.HeatTransfer.Conduction.SingleLayer` component of the Modelica Buildings Library. A modified version (`SingleLayerSlPCMlib`) is used with the transition models and media contained in slPCMlib.

As an application example, the test case 600FF of the Building Energy Simulation Test (BESTEST) validation suite (Judkoff and Neymark, 1995) is considered, as implemented in the Buildings library (Wetter et al., 2014). Case 600FF is a light-weight building with a single room

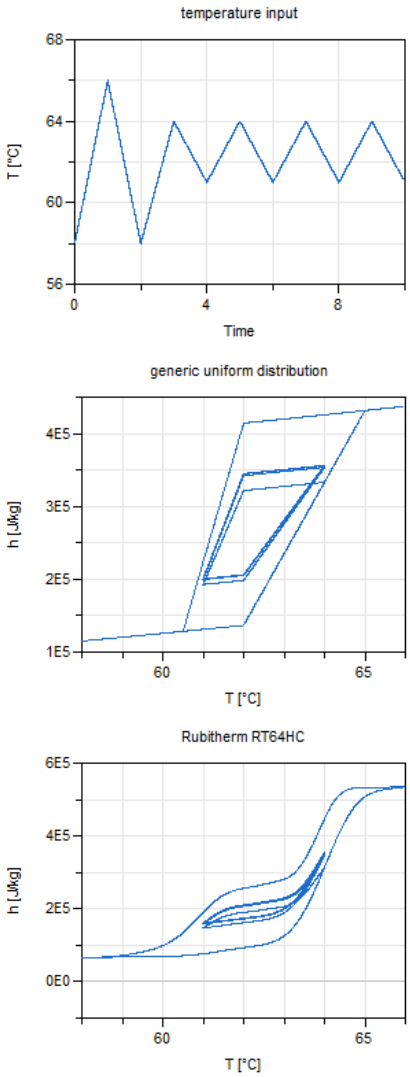

Figure 8. Periodic temperature variations (first subfigure), and the response in the enthalpy-temperature diagram computed with the "curve scale" model: for a generic PCM (second subfigure), and a specific PCM (third subfigure).

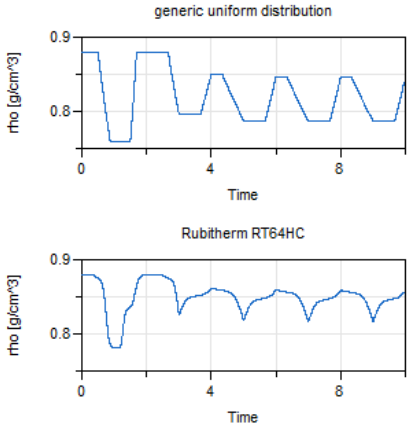

Figure 9. Density changes as response to the temperature variations in Figure 8 (first subfigure). The response is modeled with the "curve scale" model for the two PCM shown in the second and third subfigure in Figure 8.

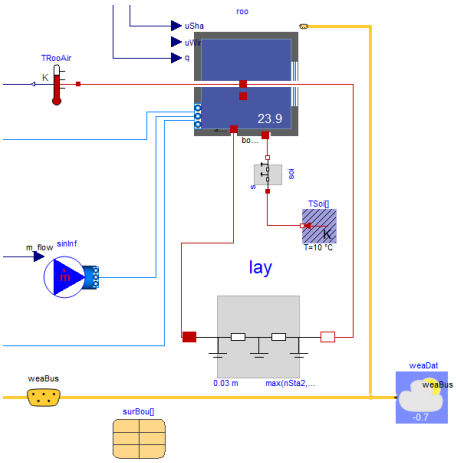

Figure 10. Test case 600FF taken from Modelica Buildings Library (Wetter et al., 2014) with a modified model for a single layer PCM wall element (lay).

of 8 m by 6 m and 2.7 m height. The room temperature is free floating. Double SB26 wall elements of $2 \cdot 15\,\text{mm}$ thickness are attached to the interior wall of the room. We take simplifying assumptions, define the total surface area as $2 \cdot (8\,\text{m} + 6\,\text{m}) \cdot 2.7\,\text{m}$, and connect one heat port of the `SingleLayer` as a heat port of surface connected to the room air and connect the other port to the heat port to air volume, see Figure 10. SB26 temperatures are approximated by two states inside the wall element. This means that two differential heat balance equations need to be solved, each using effective properties ρ, λ and $\tilde{c}$. Because the PCM is microencapsulated, temperature-dependence of ρ which can lead to volume changes, internal material velocities and convection is neglected.

Figure 11 shows results of yearly simulations for three scenarios: without wall element, and with a SB26 wall element considering either an *ideal* or a real phase change behavior. The simulation results indicate differences between all three scenarios. While the PCM wall element leads to an increase in the number of hours with temperatures between 20 and 30 °C, the ideal and real phase change behaviors result in different temperature distributions.

The CPU-times for integration are given in Table 1. As expected, the CPU-times of the test case including SB26 are increased compared with the original case (w/o SB26). The case with the *real* SB26 needs less time compared with the case with ideal SB26. This can be explained by the differences in the phase transition temperature range, i.e. narrow range of the *ideal* SB26 and wide range for the *real* SB26, with corresponding sharp and smooth changes in the apparent heat capacity (and enthalpy) curve, see the third subfigure in Figure 11. Sharp changes in thermal properties make the problem more nonlinear and thus, more difficult to solve. The temperature and climate variability over a year triggers many events when solving the hysteresis models. Interestingly enough, corresponding stops and restarts of DASSL do not heavily affect the over-

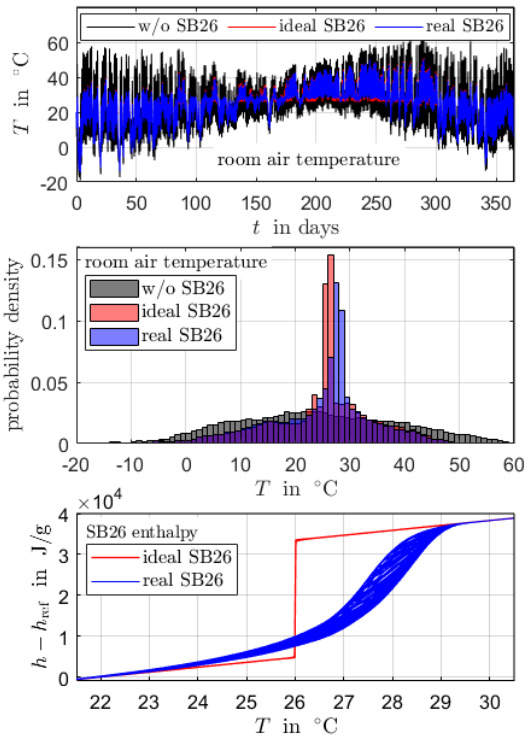

Figure 11. Test case 600FF considering the installation of a commercial PCM impregnated gypsum board SmartBoard®26 (SB26). The first and second subfigure show the temporal evolution and a histogram of the room temperature for three scenarios: without SB26 wall element; with SB26 wall element considering an ideal phase change behavior (as implemented in the Buildings Library); and with SB26 wall element considering a realistic phase change behavior identified from caloric measurements (as implemented in slPCMlib). The third subfigure shows the evolution of the SB26 specific enthalpy in the enthalpy-temperature diagram.

Table 1. CPU-time for integration of the test case 600FF. All computations were carried out on a laptop with Intel(R) Core(TM) i5-8350U CPU @ 1.70 GHz 1.90 GHz and 16 GB RAM. Parallelization of code was not used. The default solver DASSL was selected with a tolerance of 1E-6 and interval length of 60 s.

Scenario	*Model*	*Computation time*	
		absolute	*relative*
w/o SB26	-	74 s	100 %
ideal SB26	melting curve	121 s	164 %
real SB26	melting curve	88 s	119 %
real SB26	curve track	101 s	136 %
real SB26	curve switch	129 s	174 %
real SB26	curve scale	106 s	143 %

DOI
10.3384/ecp19363

all computation times. It should however be noted that the above results are not necessarily generalizable.

6 Discussion and conclusions

slPCMlib allows for a detailed analysis of the thermal performance of PCM enhanced materials and components. Compared with property models considering an isothermal phase change behavior the phase transition models in slPCMlib may be more realistic and accurate. The second application example indicates that this comes at the cost of a quite acceptable increase in model complexity and solution times.

The presented phenomenological hysteresis models are rate-independent. From a practical perspective this is an advantage: They can be easily parametrized by only two curves, e.g. considering heat capacity data from melting and solidification experiments. A comparable approach is used for parametrization of the so-called Tellinen hysteresis model (Tellinen, 1998) which predicts properties of ferromagnetic materials (Ziske and Bödrich, 2012). An interesting extension for rate-dependent modeling could be based on a model-free kinetic analysis of PCM heat capacity data, as recently proposed by Lizana et al. (2021).

In the current version of slPCMlib it is not possible to use the hysteresis models with the enthalpy method for modeling heat transfer in PCM. To do so, an inverse relation for the phase fraction-temperature (and/or enthalpy-temperature) relation would be needed. Examples can be found in literature, however, they are restricted to specific phase transition ansatz functions (and curve shapes): Huang et al. (2022) derives an analytic form of the inverse *curve scale* model parametrized with piecewise linear phase transition functions (the *generic* uniform distribution ansatz function in slPCMlib). Takacs et al. (2008) derives an inverse magnetic hysteresis model considering hyperbolic ansatz functions.

The performance (initialization and CPU-times) of the *curve switch* and *curve scale* models is significantly improved by differentiation with respect to time. However, relaxed solver tolerances may lead to incorrect results. With the current implementation the *melting curve* and *curve track* models, as well as the *curve scale* model (with reasonably strict tolerances) can be all recommended for use. Results from the *curve switch* model might need a critical validation. In any case, a plot in the enthalpy-temperature diagram is recommendable to quickly identify possible errors.

slPCMlib and the examples discussed above can be found at https://github.com/AIT-TES/slPCMlib.

7 Acknowledgement

T.B. acknowledges funding by the Energieforschung (e!MISSION) project fronTector (phase front detector, number 881143). The authors acknowledge the helpful discussion with Atiyah Elsheikh and his suggestions on how to structure the library.

References

Q. Al-Yasiri and M. Szabó. Incorporation of phase change materials into building envelope for thermal comfort and energy saving: A comprehensive analysis. *Journal of Building Engineering*, 36:102122, 2021.

T. Barz. Paraffins as phase change material in a compact plate-fin heat exchanger-Part II: Validation of the "curve scale" hysteresis model for incomplete phase transitions. *Journal of Energy Storage*, 34:102164, 2021.

T. Barz and A. Sommer. Modeling hysteresis in the phase transition of industrial-grade solid/liquid PCM for thermal energy storages. *International Journal of Heat and Mass Transfer*, 127:701–713, 2018.

T. Barz, J. Emhofer, K. Marx, G. Zsembinszki, and L.F. Cabeza. Phenomenological modelling of phase transitions with hysteresis in solid/liquid PCM. *Journal of Building Performance Simulation*, 12(6):770–788, 2019.

T. Barz, J. Krämer, and J. Emhofer. Identification of phase fraction–temperature curves from heat capacity data for numerical modeling of heat transfer in commercial paraffin waxes. *Energies*, 13(19):5149, 2020.

K. Biswas, Y. Shukla, A. Desjarlais, and R. Rawal. Thermal characterization of full-scale PCM products and numerical simulations, including hysteresis, to evaluate energy impacts in an envelope application. *Applied Thermal Engineering*, 138:501–512, 2018.

J. Bony and S. Citherlet. Numerical model and experimental validation of heat storage with phase change materials. *Energy and Buildings*, 39(10):1065–1072, 2007.

A. Buonomano and F. Guarino. The impact of thermophysical properties and hysteresis effects on the energy performance simulation of PCM wallboards: Experimental studies, modelling, and validation. *Renewable and Sustainable Energy Reviews*, 126:109807, 2020.

K. Filonenko, V.B. Ljungdahl, T. Yang, and C. Veje. Modelica implementation of phase change material ventilation unit. In *2020 6th IEEE International Energy Conference (ENERGYCon)*. IEEE, 2020.

F. Goia, G. Chaudhary, and S. Fantucci. Modeling and experimental validation of an algorithm for simulation of hysteresis effects in phase change materials for building components. *Energy and Buildings*, 174:54–67, 2018.

A. Halimov, M. Lauster, and D. Müller. Validation and integration of a latent heat storage model into building envelopes of a high-order building model for Modelica library AixLib. *Energy and Buildings*, 202:109336, 2019.

D. Helmns, D.H. Blum, S.M. Dutton, and P. van Carey. Development and validation of a latent thermal energy storage model using Modelica. *Energies*, 14(1):194, 2021.

W. Hemminger and S. Sarge. The baseline construction and its influence on the measurement of heat with differential scanning calorimeters. *Journal of Thermal Analysis and Calorimetry*, 37(7):1455–1477, 1991.

Y. Hu and P.K. Heiselberg. A new ventilated window with PCM heat exchanger—performance analysis and design optimization. *Energy and Buildings*, 169:185–194, 2018.

H. Huang, J. Lin, Q. Zhao, Z. Xie, and Y. Xiao. Numerical model of pcm heat exchange based on dynamic boundary. *Energy Reports*, 8:579–587, 2022.

Y. Ivshin and T.J. Pence. A constitutive model for hysteretic phase transition behavior. *International Journal of Engineering Science*, 32(4):681–704, 1994.

R. Judkoff and J. Neymark. International Energy Agency building energy simulation test (BESTEST) and diagnostic method. Technical Report NREL/TP-472-6231, National Renewable Energy Lab. (NREL), Golden, CO, United States, Feb 1995. URL https://www.osti.gov/biblio/90674.

J. Kośny. *PCM-Enhanced Building Components: An Application of Phase Change Materials in Building Envelopes and Internal Structures*. Engineering Materials and Processes. Springer, 2015.

F. Kuznik, D. David, K. Johannes, and J.-J. Roux. A review on phase change materials integrated in building walls. *Renewable and Sustainable Energy Reviews*, 15(1):379–391, 2011.

C. Leonhardt and D. Müller. Modelling of residential heating systems using a phase change material storage system. In *Proceedings of the 7th International Modelica Conference*, pages 507–512. Linköping University Electronic Press, 2009.

C. Lerche, H. Siegmund, K. Brands, and L. Kossack. Entwicklung eines innovativen Aktiv- Kühl- und Heizboden unter Ausnutzung des Latentspeicherprinzips. Technical Report Az: 23836 - 24/2, Deutsche Bundesstiftung Umwelt, IBB MODUL AIR KG, Germany, Bad Honnef, Germany, Oct 2010. URL https://www.dbu.de/2468.html.

J. Lizana, A. Perejón, P.E. Sanchez-Jimenez, and L.A. Perez-Maqueda. Advanced parametrisation of phase change materials through kinetic approach. *Journal of Energy Storage*, 44:103441, 2021.

J.E. McDonald. Homogeneous nucleation of supercooled water drops. *Journal of Atmospheric Sciences*, 10(6):416–433, 1953.

B. Michel, P. Glouannec, A. Fuentes, and P. Chauvelon. Experimental and numerical study of insulation walls containing a composite layer of PU-PCM and dedicated to refrigerated vehicle. *Applied Thermal Engineering*, 116:382–391, 2017.

E. Moreles, G. Huelsz, and G. Barrios. Hysteresis effects on the thermal performance of building envelope PCM-walls. *Building Simulation*, 11(3):519–531, 2018.

J. Rose, A. Lahme, N. U. Christensen, P. Heiselberg, M. Hansen, and K. Grau. Numerical method for calculating latent heat storage in constructions containing phase change material. In *Proceedings of Building Simulation 2009: 11th conference of the international building performance simulation association*, pages 400–407, 2009.

Rubitherm Technologies GmbH. PCM RT-line: Technical data sheets. https://www.rubitherm.eu/en/productCategories.html. [Online; accessed 01-December-2019].

J. Takacs, G. Kovacs, and L.K. Varga. Hysteresis reversal. *Physica B: Condensed Matter*, 403(13-16):2293–2297, 2008.

J. Tellinen. A simple scalar model for magnetic hysteresis. *IEEE Transactions on Magnetics*, 34(4):2200–2206, 1998.

V. R. Voller, C. R. Swaminathan, and B. G. Thomas. Fixed grid techniques for phase change problems: A review. *International Journal for Numerical Methods in Engineering*, 30(4): 875–898, 1990.

M. Wetter, W. Zuo, T.S. Nouidui, and X. Pang. Modelica Buildings library. *Journal of Building Performance Simulation*, 7 (4):253–270, 2014.

J. Ziske and T. Bödrich. Magnetic hysteresis models for Modelica. In *Proceedings of the 9th International MODELICA Conference*, pages 151–158. Linköping University Electronic Press, 2012.

DOI
10.3384/ecp19363